Revealing The Exotic Structure Of Molecules In Strong Magnetic Fields

Miles J. Pemberton,[1] Tom J. P. Irons,[1, a)] Trygve Helgaker,[2] and Andrew M. Teale[1, 2]

[1)] *School of Chemistry, University of Nottingham, NG7 2RD, UK*

[2)] *Hylleraas Centre for Quantum Molecular Sciences, Department of Chemistry, University of Oslo, P.O. Box 1033, Blindern, Oslo N-0315, Norway*

(Dated: 21 April 2022)

[a)] Electronic mail: tom.irons@nottingham.ac.uk

$\|\mathbf{B}\|/B_0$	Ground State	E/E_h	Lowest Energy Dissociation	ΔE / kJ mol^{-1}
0.0	$He_4^{(0)}$	-11.636889	$He_4^{(0)} \rightarrow He_3^{(0)} + He^{(0)}$	0.34
0.2	$He_4^{(0)}$	-11.604836	$He_4^{(0)} \rightarrow He_3^{(0)} + He^{(0)}$	0.41
0.4	$He_4^{(0)}$	-11.511727	$He_4^{(0)} \rightarrow He_3^{(0)} + He^{(0)}$	0.73
0.6	$He_4^{(-1)}$	-11.378963	$He_4^{(-1)} \rightarrow He_3^{(-1)} + He^{(0)}$	7.25
0.8	$He_4^{(-2)}$	-11.541239	$He_4^{(-2)} \rightarrow He_2^{(-1)} + He_2^{(-1)}$	35.17
1.0	$He_4^{(-4)}$	-11.801422	$He_4^{(-4)} \rightarrow He_3^{(-3)} + He^{(-1)}$	133.92

Table SI (a): Lowest energy He_4 dissociation pathways.

$\|\mathbf{B}\|/B_0$	Ground State	E/E_h	Lowest Energy Dissociation	ΔE / kJ mol^{-1}
0.0	$He_3^{(0)}$	-8.727618	$He_3^{(0)} \rightarrow He_2^{(0)} + He^{(0)}$	0.30
0.2	$He_3^{(0)}$	-8.703583	$He_3^{(0)} \rightarrow He_2^{(0)} + He^{(0)}$	0.42
0.4	$He_3^{(0)}$	-8.633739	$He_3^{(0)} \rightarrow He_2^{(0)} + He^{(0)}$	0.75
0.6	$He_3^{(-1)}$	-8.535540	$He_3^{(-1)} \rightarrow He_2^{(-1)} + He^{(0)}$	58.72
0.8	$He_3^{(-2)}$	-8.595461	$He_3^{(-2)} \rightarrow He_2^{(-1)} + He^{(-1)}$	37.03
1.0	$He_3^{(-3)}$	-8.830147	$He_3^{(-3)} \rightarrow He_2^{(-2)} + He^{(-1)}$	124.90

Table SI (b): Lowest energy He_3 dissociation pathways.

I. LOWEST ENERGY HE_n DISSOCIATION PATHWAYS

Lowest energy dissociation pathways and their associated energies computed using CDFT with the cTPSS functional and aug-cc-pVTZ orbital basis set for the ground-state He_n (n = 2-4) structures at $|\mathbf{B}|$ = 0.0-1.0 B_0 in increments of 0.2 B_0, calculated from the energies of the He_n clusters and the relevant smaller fragments obtained from the AIRSS analysis for these systems.

II. LOWEST ENERGY CH_n DISSOCIATION PATHWAYS

Lowest energy dissociation pathways and their associated energies computed using CDFT with the cTPSS functional and aug-cc-pVTZ orbital basis set for the ground-state CH_n (n

$\|\mathbf{B}\|/B_0$	Ground State	E/E_h	Lowest Energy Dissociation	ΔE / kJ mol^{-1}
0.0	$He_2^{(0)}$	-5.818360	$He_2^{(0)} \rightarrow He^{(0)} + He^{(0)}$	0.20
0.2	$He_2^{(0)}$	-5.802316	$He_2^{(0)} \rightarrow He^{(0)} + He^{(0)}$	0.32
0.4	$He_2^{(0)}$	-5.755667	$He_2^{(0)} \rightarrow He^{(0)} + He^{(0)}$	0.65
0.6	$He_2^{(0)}$	-5.681800	$He_2^{(0)} \rightarrow He^{(0)} + He^{(0)}$	1.27
0.8	$He_2^{(-1)}$	-5.763922	$He_2^{(-1)} \rightarrow He^{(-1)} + He^{(0)}$	406.00
1.0	$He_2^{(-2)}$	-5.862310	$He_2^{(-2)} \rightarrow He^{(-1)} + He^{(-1)}$	57.18

Table SI (c): Lowest energy He_2 dissociation pathways.

$\|\mathbf{B}\|/B_0$	Ground State	E/E_h	Lowest Energy Dissociation	ΔE / kJ mol^{-1}
0.0	$CH_3^{(-1/2)}$	-39.864710	$CH_3^{(-1/2)} \rightarrow CH^{(-1/2)} + H_2^{(0)}$	475.0
0.2	$CH_3^{(-3/2)}$	-39.932304	$CH_3^{(-3/2)} \rightarrow CH_2^{(-1)} + H^{(-1/2)}$	4.52
0.4	$CH_3^{(-7/2)}$	-40.325536	$CH_3^{(-7/2)} \rightarrow CH_2^{(-3)} + H^{(-1/2)}$	3.84
0.6	$CH_3^{(-7/2)}$	-40.812574	$CH_3^{(-7/2)} \rightarrow CH_2^{(-3)} + H^{(-1/2)}$	34.80
0.8	$CH_3^{(-7/2)}$	-41.308903	$CH_3^{(-7/2)} \rightarrow CH_2^{(-3)} + H^{(-1/2)}$	43.43
1.0	$CH_3^{(-7/2)}$	-41.757455	$CH_3^{(-7/2)} \rightarrow CH_2^{(-3)} + H^{(-1/2)}$	50.16

Table SII (a): Lowest energy CH_3 dissociation pathways.

= 1-3) structures at $|\mathbf{B}|$ = 0.0-1.0 B_0 in increments of 0.2 B_0, calculated from the energies of the CH_n clusters and the relevant smaller fragments obtained from the AIRSS analysis for these systems.

III. CONVEX HULL PLOTS FOR HE_n WITH CTPSS

Convex hull plots for He_n (n = 2 - 4) showing the optimised energies obtained from random initial structures of He_n with the corresponding M_s values in magnetic fields of 0.0-1.0 B_0 at intervals of 0.2 B_0, computed using CDFT with the cTPSS functional and aug-cc-pVTZ orbital basis set. The lowest energy structures of each spin-projection from $|\mathbf{B}|$ = 0.0-1.0 B_0 form a convex hull, shown by the dashed lines.

$\lvert\mathbf{B}\rvert/B_0$	Ground State	E/E_h	Lowest Energy Dissociation	ΔE / kJ mol^{-1}
0.0	$CH_2^{(-1)}$	-39.181056	$CH_2^{(-1)} \rightarrow C^{(-1)} + H_2^{(0)}$	375.65
0.2	$CH_2^{(-1)}$	-39.340526	$CH_2^{(-1)} \rightarrow C^{(-1)} + H_2^{(0)}$	159.42
0.4	$CH_2^{(-3)}$	-39.660549	$CH_2^{(-3)} \rightarrow CH^{(-5/2)} + H^{(-1/2)}$	4.30
0.6	$CH_2^{(-3)}$	-40.073504	$CH_2^{(-3)} \rightarrow CH^{(-5/2)} + H^{(-1/2)}$	37.32
0.8	$CH_2^{(-3)}$	-40.511763	$CH_2^{(-3)} \rightarrow CH^{(-5/2)} + H^{(-1/2)}$	42.28
1.0	$CH_2^{(-3)}$	-40.908811	$CH_2^{(-3)} \rightarrow CH^{(-5/2)} + H^{(-1/2)}$	46.36

Table SII (b): Lowest energy CH_2 dissociation pathways.

$\lvert\mathbf{B}\rvert/B_0$	Ground State	E/E_h	Lowest Energy Dissociation	ΔE / kJ mol^{-1}
0.0	$CH^{(-1/2)}$	-38.503919	$CH^{(-1/2)} \rightarrow C^{(0)} + H^{(-1/2)}$	546.23
0.2	$CH^{(-3/2)}$	-38.726099	$CH^{(-3/2)} \rightarrow C^{(-1)} + H^{(-1/2)}$	55.60
0.4	$CH^{(-5/2)}$	-38.995386	$CH^{(-5/2)} \rightarrow C^{(-2)} + H^{(-1/2)}$	3.59
0.6	$CH^{(-5/2)}$	-39.333473	$CH^{(-5/2)} \rightarrow C^{(-2)} + H^{(-1/2)}$	39.44
0.8	$CH^{(-5/2)}$	-39.715062	$CH^{(-5/2)} \rightarrow C^{(-2)} + H^{(-1/2)}$	32.40
1.0	$CH^{(-5/2)}$	-40.061617	$CH^{(-5/2)} \rightarrow C^{(-2)} + H^{(-1/2)}$	30.07

Table SII (c): Lowest energy CH dissociation pathways.

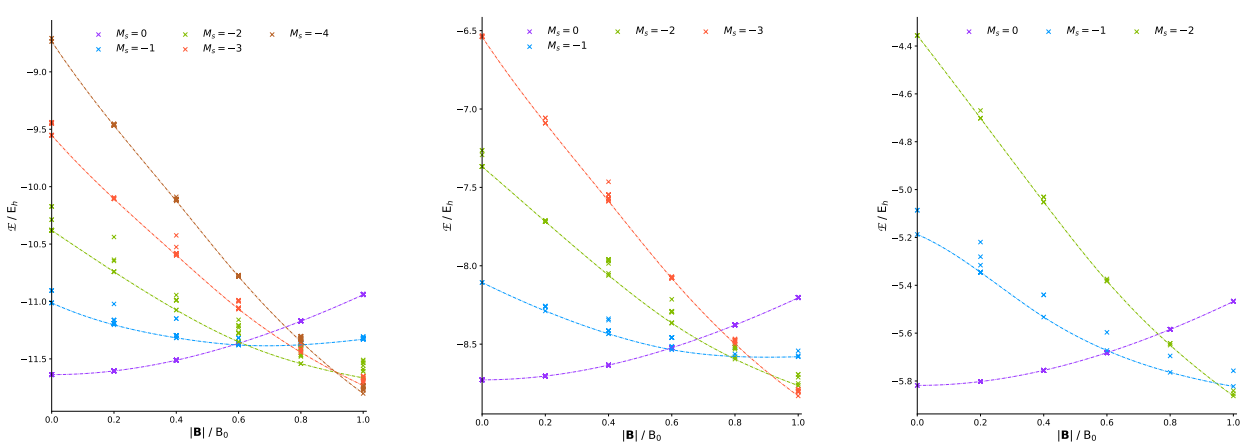

(a) He_4 (b) He_3 (c) He_2

Figure SI: He_n (n = 2 - 4) cluster cTPSS convex hull plots.

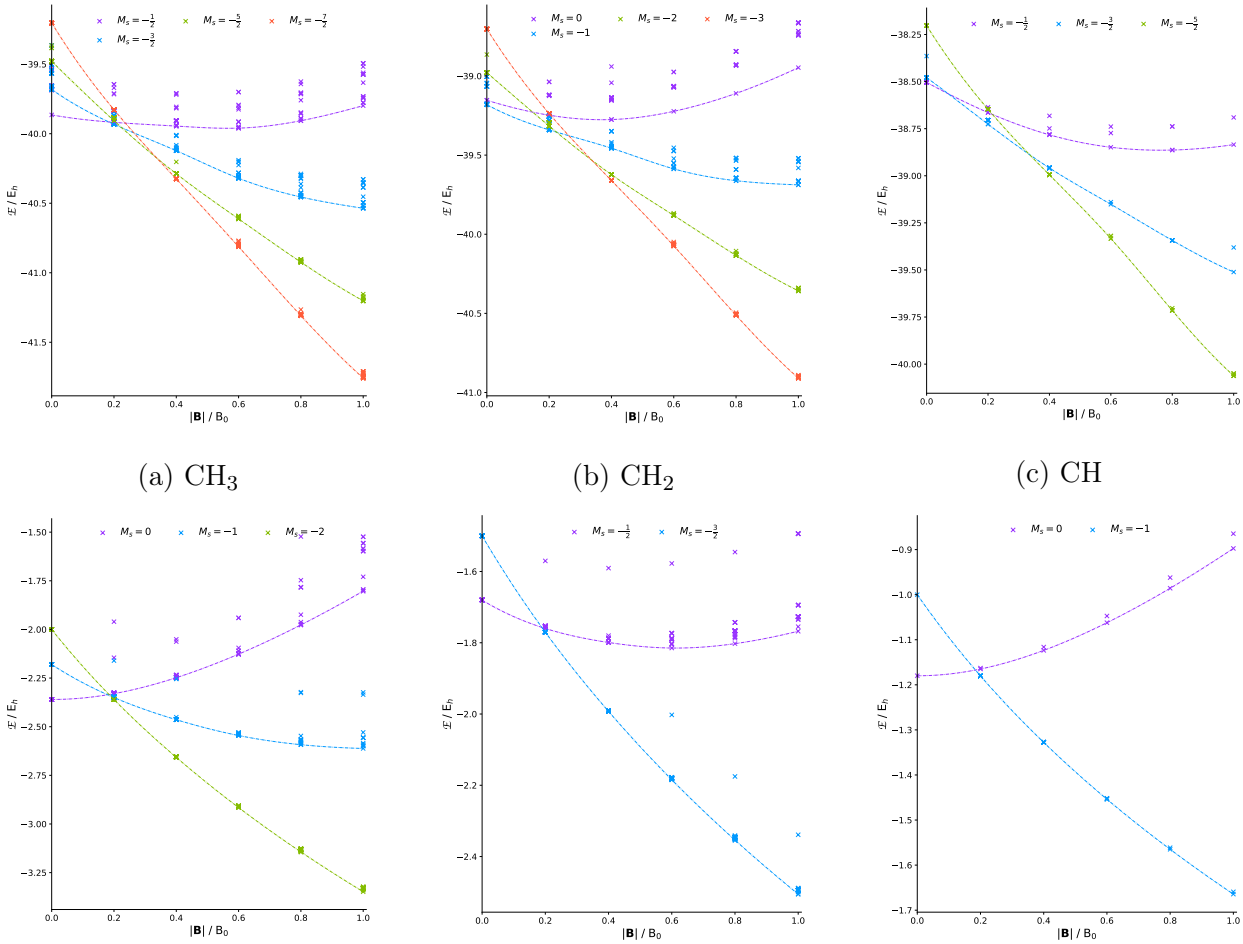

(a) CH_3 (b) CH_2 (c) CH

(d) H_4 (e) H_3 (f) H_2

Figure SII: CH_n and H_n cTPSS convex hull plots.

IV. CONVEX HULL PLOTS FOR CH_n & H_n WITH CTPSS

Convex hull plots for CH_n (n = 1 - 3) and H_n (n = 2 - 4) showing the optimised energies obtained from random initial structures of CH_n and H_n with the corresponding M_s values in magnetic fields of 0.0-1.0 B_0 at intervals of 0.2 B_0, computed using CDFT with the cTPSS functional and aug-cc-pVTZ orbital basis set. The lowest energy structures of each spin-projection from $|\mathbf{B}|$ = 0.0-1.0 B_0 form a convex hull, shown by the dashed lines.

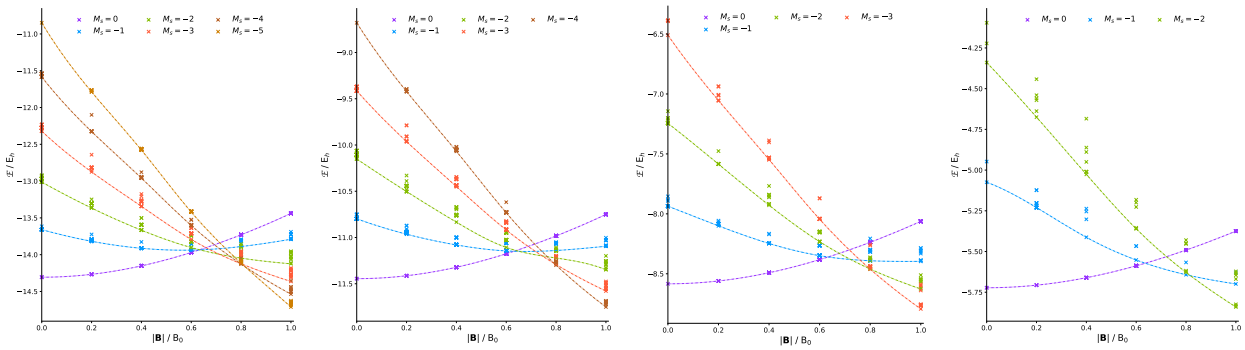

(a) He_5 (b) He_4 (c) He_3 (d) He_2

Figure SIII: He_n (n = 2 - 5) cluster HF convex hull plots.

V. CONVEX HULL PLOTS FOR HE_n WITH HF

Convex hull plots for He_n (n = 2 - 5) showing the optimised energies obtained from random initial structures of He_n with the corresponding M_s values in magnetic fields of 0.0-1.0 B_0 at intervals of 0.2 B_0, computed using HF and the aug-cc-pVTZ orbital basis set. The lowest energy structures of each spin-projection from $|\mathbf{B}|$ = 0.0-1.0 B_0 form a convex hull, shown by the dashed lines.

VI. CONVEX HULL PLOTS FOR CH_n WITH HF

Convex hull plots for CH_n (n = 1 - 4) showing the optimised energies obtained from random initial structures of CH_n with the corresponding M_s values in magnetic fields of 0.0-1.0 B_0 at intervals of 0.2 B_0, computed using HF and the aug-cc-pVTZ orbital basis set. The lowest energy structures of each spin-projection from $|\mathbf{B}|$ = 0.0-1.0 B_0 form a convex hull, shown by the dashed lines.

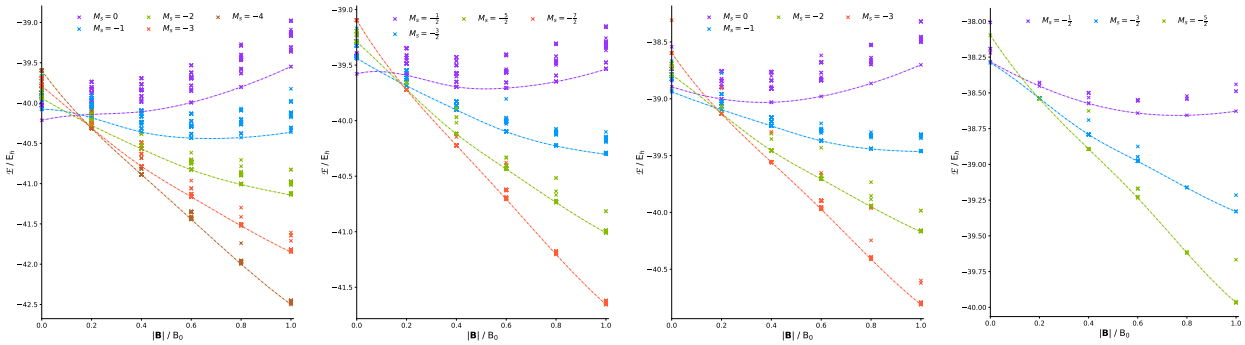

(a) CH_4 (b) CH_3 (c) CH_2 (d) CH

Figure SIV: CH_n HF convex hull plots.